OXFORD

Human Molecular Genetics, 2015, Vol. 24, No. 11 3206–3219

doi: 10.1093/hmg/ddv072
Advance Access Publication Date: 20 February 2015
Original Article

ORIGINAL ARTICLE

A genetic dissection of intestinal fat-soluble vitamin and carotenoid absorption

M. Airanthi K. Widjaja-Adhi, Glenn P. Lobo, Marcin Golczak and Johannes Von Lintig*

Department of Pharmacology, School of Medicine, Case Western Reserve University, 10900 Euclid Avenue, Cleveland, OH 44106, USA

*To whom correspondence should be addressed. Tel: +1 2163683528; Fax: +1 2163681300; Email: johannes.vonlintig@case.edu

Abstract

Carotenoids are currently investigated regarding their potential to lower the risk of chronic disease and to combat vitamin A deficiency. Surprisingly, responses to dietary supplementation with these compounds are quite variable between individuals. Genome-wide studies have associated common genetic polymorphisms in the *BCO1* gene with this variability. The *BCO1* gene encodes an enzyme that is expressed in the intestine and converts provitamin A carotenoids to vitamin A-aldehyde. However, it is not clear how this enzyme can impact the bioavailability and metabolism of other carotenoids such as xanthophyll. We here provide evidence that BCO1 is a key component of a regulatory network that controls the absorption of carotenoids and fat-soluble vitamins. In this process, conversion of β-carotene to vitamin A by BCO1 induces via retinoid signaling the expression of the intestinal homeobox transcription factor ISX. Subsequently, ISX binds to conserved DNA-binding motifs upstream of the *BCO1* and *SCARB1* genes. SCARB1 encodes a membrane protein that facilitates absorption of fat-soluble vitamins and carotenoids. In keeping with its role as a transcriptional repressor, SCARB1 protein levels are significantly increased in the intestine of ISX-deficient mice. This increase results in augmented absorption and tissue accumulation of xanthophyll carotenoids and tocopherols. Our study shows that fat-soluble vitamin and carotenoid absorption is controlled by a BCO1-dependent negative feedback regulation. Thus, our findings provide a molecular framework for the controversial relationship between genetics and fat-soluble vitamin status in the human population.

Introduction

Carotenoids affect a rich variety of physiological functions in nature and are beneficial for human health (1). For instance, the xanthophyll carotenoids lutein, zeaxanthin and *meso*-zeaxanthin accumulate in the *macula lutea* of the primate eyes (2–5) where they protect the retina against damaging stress by their antioxidant and light-filtering properties (6,7). Additionally, carotenoids serve as precursors for apocarotenoid cleavage products, including retinoids (vitamin A and its derivatives) (8,9).

Low carotenoid status, especially blood and tissue levels of xanthophylls, has been associated with a number of degenerative diseases such as cardiovascular disease, cognitive impairments and the age-related macular degeneration (AMD) (6,10–13). Studies indicating that zeaxanthin and lutein can reduce the risk and progression of AMD have attracted broad clinical interest (11,14–16). Surprisingly, plasma and tissue levels of carotenoids are only weakly correlated with dietary intake (17–19). Genome-wide and candidate gene association studies have identified single-nucleotide polymorphisms (SNPs) in *BCO1* gene to be correlated with this variability (20–24). The *BCO1* gene (also known as *BCMO1* gene) encodes a β-carotene-15,15′-dioxygenase that converts provitamin A carotenoids into retinaldehyde (vitamin A-aldehyde) (25–28). From the primary cleavage products, all biologically active retinoids can be synthesized including the visual chromophore (11-*cis*-retinal) and the vitamin A hormone (all-*trans*-retinoic acid) (29). The enzyme localizes to the cytoplasm and is expressed in the intestine and various

Received: January 5, 2015. **Revised and Accepted:** February 18, 2015

other tissues (30,31). Intervention studies in female volunteers suggest that carriers of the SNPs display altered conversion rates of absorbed dietary β-carotene to vitamin A (32). However, how BCO1 affects the bioavailability and metabolism of xanthophylls such as zeaxanthin and lutein that are not substrates of the enzyme remains elusive.

Carotenoids are absorbed in the intestine and together with other dietary lipids delivered to the organism as triglyceride-rich lipoproteins. Carotenoids interact at many stages of this transport process (33). Thus, the association between BCO1 and xanthophyll homeostasis may be mediated by an indirect effect of provitamin A. Recently, we reported that intestinal vitamin A production is under negative feedback regulation (34,35). In this regulatory process, retinoic acid via retinoic acid receptors (RARs) induces the expression of the intestine-specific homeobox transcription factor ISX. In turn, ISX binds to a conserved DNA-binding motif upstream of the *BCO1* gene and suppresses the intestinal expression of the vitamin A-forming enzyme (35). Besides *BCO1*, ISX also controls the expression levels of the gene encoding the scavenger receptor class B Type 1 (SCARB1) in the intestine (34,36). The SCARB1 protein localizes to the membranes of the apical surface of absorptive epithelial cells, and its levels decrease from the duodenum to ileum (37,38). This receptor facilitates the intestinal absorption of various essential dietary lipids including carotenoids and fat-soluble vitamins [for recent review, see (39)]. Thus, BCO1 activity via ISX signaling could control SCARB1 activity and be a critical modulator of carotenoid and fat-soluble vitamin absorption in the intestine (Fig. 1).

To test this hypothesis, we employed the β-carotene-9,10-dioxygenase deficient ($Bco2^{-/-}$) mouse model recently generated in our laboratory (40). This enzyme resides in the inner membrane of mitochondria (41) and was initially cloned from mouse, human and zebrafish (42). Biochemical studies with the recombinant enzyme from mouse and ferret revealed that BCO2 displays a broad substrate specificity and converts the carotenes, β-carotene and lycopene as well as the xanthophylls, zeaxanthin and lutein to apocarotenoid products (40,43,44). Accordingly, BCO2-deficient mice accumulate xanthophylls in plasma and peripheral tissues including the retina (40,45). To study xanthophyll absorption and body distribution, we crossed the *Bco2* knockout allele into the genetic background of the previously described $Scarb1^{-/-}$ (46), $Isx^{-/-}$ (36) and $Bco1^{-/-}$ (47) mouse lines. Our analyses in respective single and compound mouse mutants revealed that BCO1 is a key component of a diet-responsive regulatory network that controls intestinal *SCARB1* expression and the absorption of carotenoids and other lipid-soluble antioxidants.

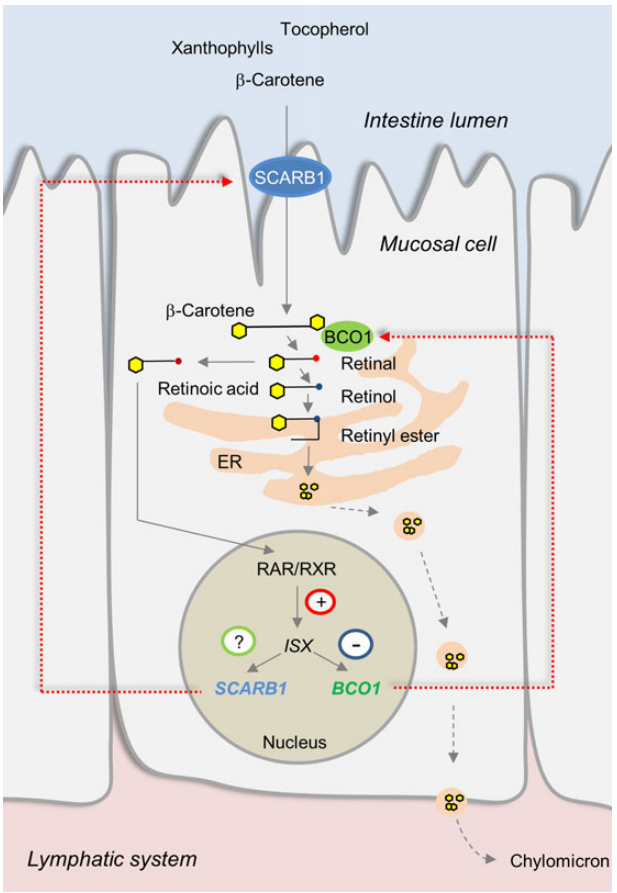

Figure 1. Scheme of the putative regulation of intestinal fat-soluble vitamin and carotenoid absorption by retinoid and ISX signaling. In this process, SCARB1 facilitates the absorption of fat-soluble vitamins and carotenoids. Absorbed β-carotene is converted to retinal by the enzyme BCO1. Retinal is either converted to retinyl esters or retinoic acid. Retinyl esters together with fat-soluble vitamins and carotenoids are packaged into chylomicrons for secretion into the lymph. Retinoid acid via retinoid acid receptor signaling (RAR/RXR) induces the expression of the intestine-specific homeobox transcription factor ISX. ISX is a transcriptional repressor and binds to elements upstream of the *BCO1* and *SCARB1* genes.

Results

SCARB1 facilitates zeaxanthin uptake and is an ISX target gene

Previous studies suggest that SCARB1 facilitates the intestinal absorption of various essential dietary lipids including β-carotene and tocopherols (39,48,49). However, direct *in vivo* evidence that SCARB1 facilitates the uptake of xanthophylls is yet to be provided. Thus, we established $Scarb1^{-/-}/Bco2^{-/-}$ compound mutant mice by appropriate crossings. We subjected these mice and $Bco2^{-/-}$ single mutant control mice to dietary intervention with zeaxanthin (150 mg/kg). We chose zeaxanthin as a model xanthophyll for our studies because mice express a zeaxanthin-binding protein that may help sequester this lipid in peripheral tissues including the retina (45). After 10 weeks, mice were sacrificed and serum and liver were collected. HPLC analysis revealed that $Scarb1^{-/-}/Bco2^{-/-}$ compound mutant mice displayed significantly lower levels (8-fold and 2-fold in the liver and serum, respectively) when compared with $Bco2^{-/-}$ single mutant mice (Fig. 2A), indicating that SCARB1 is required for xanthophyll uptake. As previously described zeaxanthin underwent oxidation and existed in the form of its 3,3′-didehydro-derivative in mice (40).

The transcription factor ISX has been indicated as key regulator of intestinal *SCARB1* mRNA expression (36). To provide evidence for such a role of ISX, we employed the previously published $Isx^{-/-}$ and $Bco2^{-/-}$ mouse models (36,40) and established $Isx^{-/-}/Bco2^{-/-}$ compound mutant mice by conventional cross-breeding. Sex- and age-matched mice were then subjected to a vitamin A-sufficient diet (4000 IU vitamin A/kg diet) that contained zeaxanthin (50 mg/kg). Throughout the experimental period of 10 weeks, no significant differences were observed between genotypes in food intake and/or weight gain. After 10 weeks, mice were sacrificed and serum and tissues were collected for further analyses. We first analyzed by immunoblot analysis how intestinal SCARB1 protein levels were affected by different genotypes. For this purpose, we prepared protein extracts from

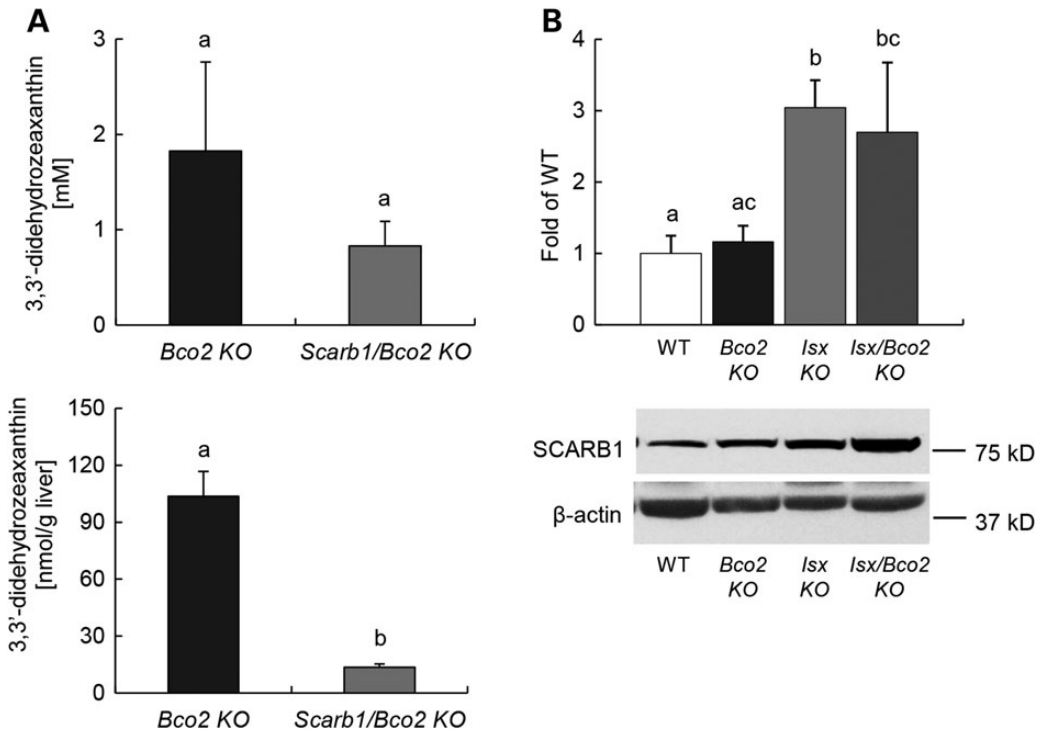

Figure 2. SCARB1 facilitate intestinal xanthophyll uptake, and its expression is regulated by ISX. (**A**) Serum (top) and hepatic (bottom) levels of 3,3′-didehydrozeaxanthin in *Bco2*$^{-/-}$ and *Scarb1*$^{-/-}$/*Bco2*$^{-/-}$ mice fed a zeaxanthin diet free of preformed vitamin A for 10 weeks. (**B**) Total protein of different mice genotype under zeaxanthin diets was obtained from jejunum and subjected to immunoblot analysis and subsequently probed with SCARB1 antibodies. Values indicate means ± SD of three female mice per genotype. Mean with different letters (a to c) differ significantly. Statistical significance was assessed by ANOVA followed by Scheffe tests using software origin 9 , with threshold of significance set at $P < 0.05$.

the jejunum of different mice. This analysis demonstrated that intestinal SCARB1 protein levels were ~3-fold higher in ISX-deficient mice (*Isx*$^{-/-}$ single and *Isx*$^{-/-}$/*Bco2*$^{-/-}$ compound mutants) when compared with ISX-sufficient mice [*Bco2*$^{-/-}$ single mutant and wild-type (wt) mice] (Fig. 2B).

We next wondered whether the interaction between ISX and the *SCARB1* gene occurred via direct protein–DNA interaction. Thus, we searched the *SCARB1* promoter for the ISX-binding motif that we previously identified in the *BCO1* gene (35). This analysis identified a 30-bp-long region ~5 kb upstream of the translational start site of the *SCARB1* gene (Fig. 3A). This putative ISX-binding region upstream of *SCARB1* gene shared 70% sequence identity with the ISX-binding motif upstream of the *BCO1* gene (Fig. 3A). The core ISX-binding sequence (8 bp) was completely conserved in both regions (Fig. 3A, underlined). To test whether ISX binds to this DNA sequence, we performed electrophoresis mobility shift assay (EMSA). We tested biotin-labeled DNA fragments containing the putative ISX-binding motif (fragment 2) or the upstream and downstream flanking DNA regions (fragments 1 and 3). These experiments revealed that recombinant ISX protein bound specifically to fragment 2 that harbored the ISX-binding motif. No binding was observed with fragments 1 and 3 (Fig. 3B). To confirm that the binding of ISX to DNA fragment 2 was specific, we added a molar excess of unlabeled fragment 2 as competitor. Almost complete competition was observed at 200-fold molar excess of the none-labeled DNA fragment (Fig. 3B, far right lane). To further confirm the specificity of ISX binding, we incubated the biotin-labeled fragment 2 with a molar excess of unlabeled DNA containing the ISX-binding motif of the murine *BCO1* gene (35). Again, the unlabeled DNA fragment competed for binding of ISX protein, indicating that ISX binding to DNA fragment 2 depends on the identified motif (Fig. 3C, Lanes 7 and 8).

The *Isx* genotype impacts zeaxanthin absorption

Next, we determined the effect of the *ISX* genotype on zeaxanthin serum and tissue levels in different mouse lines. HPLC analysis revealed that *Isx*$^{-/-}$ and *Bco2*$^{-/-}$ single mutant as well as *Isx*$^{-/-}$/*Bco2*$^{-/-}$ compound mutant mice displayed higher carotenoid serum levels when compared with wt mice (Fig. 4A). Interestingly, parent zeaxanthin was the major compound in serum of *Isx*$^{-/-}$ mice, whereas 3,3′-didehydrozeaxanthin was the predominant form of this xanthophyll in *Bco2*$^{-/-}$ and *Isx*$^{-/-}$/*Bco2*$^{-/-}$ mice. When we analyzed the livers, only *Bco2*$^{-/-}$ and *Isx*$^{-/-}$/*Bco2*$^{-/-}$ mice accumulated large amounts of zeaxanthin in the form of 3,3′-didehydro-derivative. Despite high serum levels of zeaxanthin, no hepatic accumulation of xanthophyll was found in *Isx*$^{-/-}$ mice. These mice displayed similar low levels of hepatic carotenoid levels as wt mice (Fig. 4B). Thus, we concluded that zeaxanthin absorption into the circulation is enhanced in ISX deficiency through increased intestinal SCARB1 expression. Tissue accumulation of this xanthophyll, however, only occurred in BCO2 deficiency and was accompanied by the oxidation of the parent zeaxanthin to its 3,3′-didehydro-derivative. Accordingly, *Isx*$^{-/-}$/*Bco2*$^{-/-}$ compound mutant mice with enhanced absorption and tissue accumulation showed the highest levels of hepatic xanthophylls. Similar results were found when we analyzed the gonadal white adipose tissue (WAT) (Fig. 5A). However, additional peaks beside the previously identified metabolite: 3,3′-didehydrozeaxanthin (40) appeared in the chromatogram. We performed LC–MS/MS analyses to identify the chemical identity of

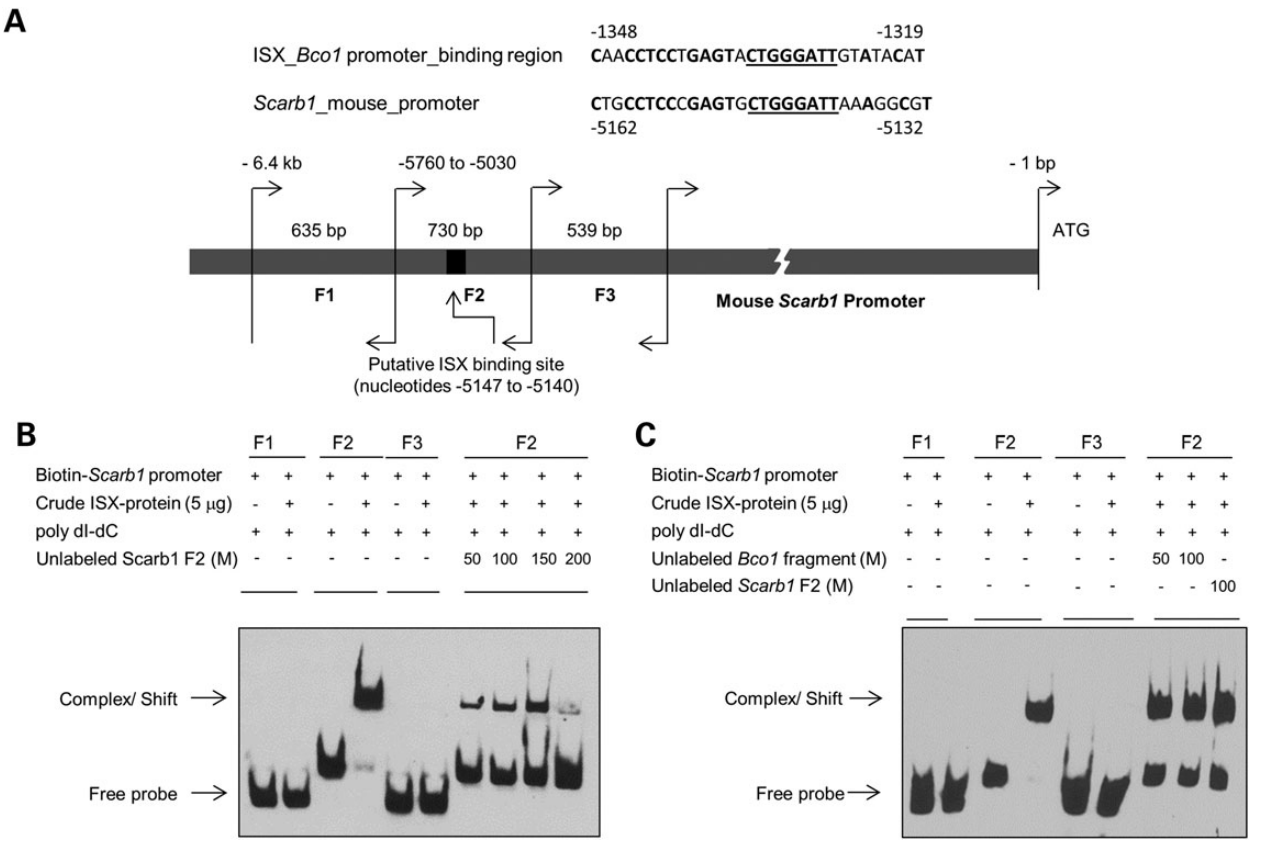

Figure 3. ISX protein binds to the *SCARB1* promoter fragment. (**A**) The mouse *SCARB1* gene is flanked by a putative ISX-binding site, which shows ~70% sequence homology to the previously identified ISX-binding site upstream if the *BCO1* gene. Nucleotide sequence similarities between the putative ISX-binding sites upstream of the *BCO1* and *SCARB1* genes are underlined. Genomic DNA was isolated from mouse intestine and using primer pairs listed in Materials and Methods. Three overlapping fragments (F1–F3) were amplified as indicated in Materials and Method. Individual DNA fragment sizes ranged from ~540 to 730 bp. The 8-bp core ISX-binding nucleotide sequence within fragment 2 (−5147 to −5140) is underlined. Individual *SCARB1* fragment sizes and positions are given relevant to the *SCARB1* ATG start site. (**B** and **C**), in EMSA, individual biotin-labeled *SCARB1* fragments were incubated with supernatant protein fraction of BL21 cells that expressed recombinant ISX. *SCARB1* fragment F2 shifted in the presence of protein extracts containing ISX protein as indicated by the arrow. No such shift in electro-mobility was observed with fragments 1 and 3 (F1 and F3). Unlabeled *SCARB1* fragment 2 [50–200 molar (M) excess] competed with the ISX binding, as shown in the right most lanes of the EMSA gels. Unlabeled *SCARB1* fragment 2 and/ or unlabeled *BCO1* fragment containing the previously identified ISX-binding nucleotide sequence competed with ISX binding to labeled *SCARB1* fragment 2. M represents molar excess concentrations of unlabeled fragments as indicated. In all EMSAs, biotin-labeled *SCARB1* promoter fragments (±ISX protein) were resolved on 6% PAGE gels, and labeled fragments were visualized by chemo-luminescence. The figures shown are representatives of images from at least two independent experiments using different ISX protein crude extract preparations.

these compounds. These zeaxanthin metabolites had a molecular mass of 562.33 Da ($m/z = 563.33$ MH^+) and thus had lost six mass units when compared with parent zeaxanthin. Based on the characteristic absorbance spectrum and molecular mass (50), they were identified as 3,3′-didehydro-4,5′-retro-zeaxanthin (Fig. 5B). This newly identified zeaxanthin metabolite displayed identical spectral characteristics and molecular mass as rhodoxanthin. This carotenoid has been previously described in several birds and fishes (50).Thus, zeaxanthin, after being fed to mice, went through further metabolic transformations (retro rearrangement and oxidation) in WAT resulting in rhodoxanthin production.

BCO1 controls xanthophyll absorption

SNPs in the human *BCO1* gene have been associated with circulating carotenoid levels and macular pigment optical density (20–22). This association could be explained by a responsiveness of carotenoid absorption to diet (34). In this process, BCO1-dependent retinoid production via retinoid signaling may impact intestinal *ISX* mRNA expression. In turn, ISX would suppress SCARB1 activity and carotenoid absorption. To test this putative interaction, we employed *Bco1*$^{-/-}$ and *Bco2*$^{-/-}$ mice as well as the corresponding compound mutant mice (*Bco1*$^{-/-}$/*Bco2*$^{-/-}$) (51). Age- and sex-matched animals were fed a diet that contained both zeaxanthin and β-carotene (75 and 25 mg/kg for each carotenoid, respectively). Except for β-carotene, the diet contained no other source for vitamin A. After 10 weeks, mice were sacrificed and serum and tissues were collected. HPLC analysis revealed that serum and liver levels of β-carotene were highest in *Bco1*$^{-/-}$ single and *Bco1*$^{-/-}$/*Bco2*$^{-/-}$ compound mutant mice (Fig. 6A), indicating that β-carotene accumulated in a BCO1-dependent fashion. HPLC analyses for zeaxanthin showed that this xanthophyll accumulated BCO2 dependently (Fig. 6B). These findings confirmed that BCO1 and BCO2 are the major metabolizing enzymes for β-carotene and zeaxanthin, respectively. The genetic inactivation of both the *BCO1* and *BCO2* genes had a striking effect on zeaxanthin accumulation. The compound mutant mice displayed ~12- and 8-fold higher levels of xanthophylls than the *BCO2* single mutant mice in serum and liver, respectively (Fig. 6B). The effect of *BCO1* genotype on xanthophyll accumulation could be explained by the conversion of

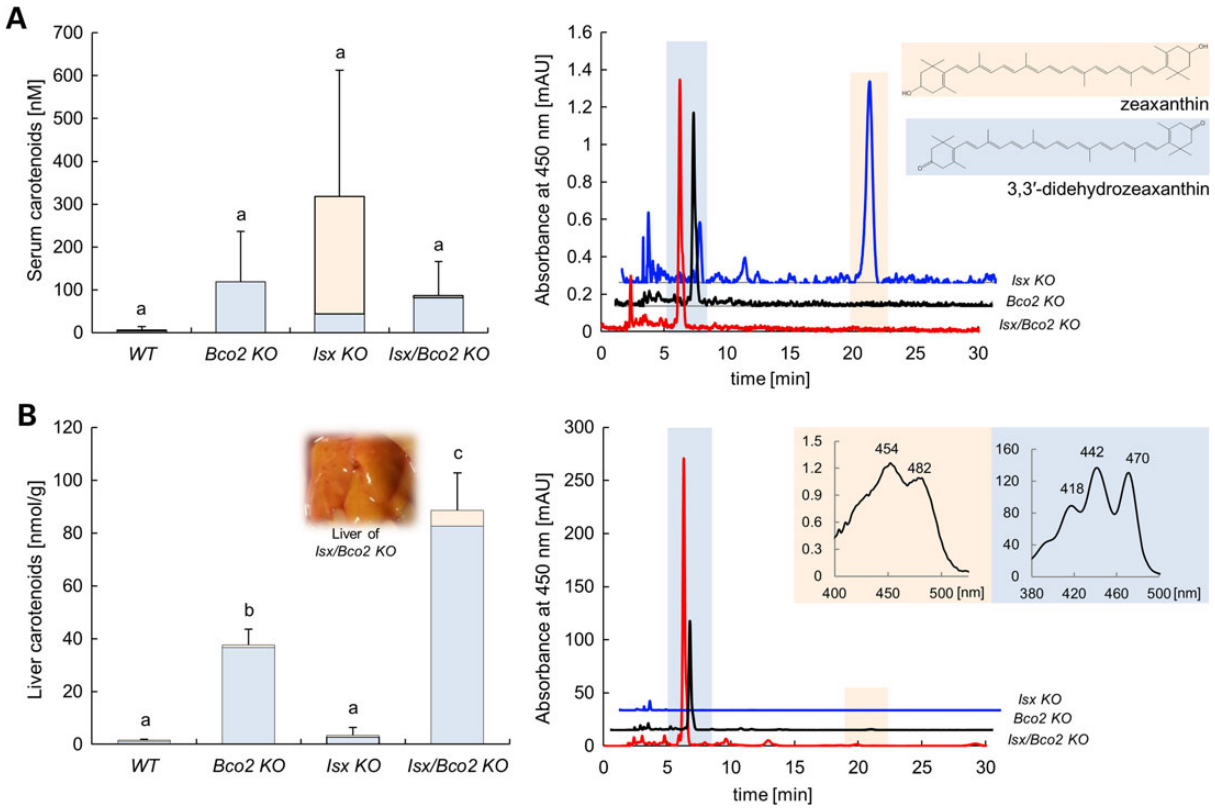

Figure 4. *ISX* genotype impacts zeaxanthin absorption. Wild type, $Bco2^{-/-}$, $Isx^{-/-}$, and $Isx^{-/-}/Bco2^{-/-}$ mice were fed for 10 weeks a zeaxanthin diet based on AIN93G. (**A**) Serum levels of 3,3′-didehydrozeaxanthin (blue bars) and parent zeaxanthin (orange bars) (left). HPLC profile at 450 nm of serum extracts from $Bco2^{-/-}$ (black line), $Isx^{-/-}$ (blue line) and $Isx^{-/-}/Bco2^{-/-}$ (red line). The inset shows the chemical structure of 3,3′-didehydrozeaxanthin (blue highlight) and parent zeaxanthin (orange highlight) (right). (**B**) Hepatic levels of 3,3′-didehydrozeaxanthin (blue bars) and parent zeaxanthin (orange bars). The inset shows the liver of $Isx^{-/-}/Bco2^{-/-}$ mice (left). HPLC profile at 450 nm of hepatic lipid extracts from $Bco2^{-/-}$ (black line), $Isx^{-/-}$ (blue line) and $Isx^{-/-}/Bco2^{-/-}$ (red line). The inset reveals the spectral characteristics of the 3,3′-didehydrozeaxanthin (blue highlight) peak and parent zeaxanthin (orange highlight) peak (right). Values indicate means ± SD from at least five female mice per serum or tissue and genotype. Mean with different letters (a to c) differ significantly. Statistical significance was assessed by one-way ANOVA followed by Scheffe tests using software origin 9, with threshold of significance set at $P < 0.01$.

β-carotene to retinoids. In turn, retinoids induce ISX expression that suppresses intestinal *SCARB1* expression and carotenoid absorption. Hence, we prepared protein extract from the jejunum of different mouse strains and performed immunoblot analysis for ISX and SCARB1. This analysis revealed that the protein levels of ISX were BCO1 dependently increased, and on the contrary, SCARB1 protein levels were BCO1 dependently decreased (Fig. 6C). Thus, we provided evidence that intestinal BCO1 activity impacts intestinal zeaxanthin absorption via retinoid and ISX signaling.

The *ISX* genotype affects fat-soluble vitamin status more generally

Evidence has been provided that SCARB1 also facilitates the intestinal absorption of other fat-soluble vitamins including tocopherols (39,49). Additionally, intestinal overexpression of SCARB1 in a transgenic mouse model revealed increased absorption of dietary lipids including fatty acids and cholesterol (52). As ISX controls intestinal SCARB1 activity, we next analyzed whether ISX deficiency affected fat-soluble vitamins and lipid status more generally. For this purpose, we analyzed wt, $Bco2^{-/-}$, $Isx^{-/-}$ and $Isx^{-/-}/Bco2^{-/-}$ mice raised on a AIN93G diet containing 75 IU vitamin E/kg diet supplemented or not supplemented with zeaxanthin (50 mg/kg). Consistent with the ISX-dependent suppression of intestinal SCARB1 gene expression, the hepatic α-tocopherol was about 2-fold elevated in compound mutant mice when compared with wt mice (Fig. 7A). The *Isx* single-knockout mice also displayed higher levels but less pronounced than in compound mutant mice. This difference in α-tocopherol levels was not dependent on zeaxanthin status of the diet. Accordingly, SCARB1 protein was also ISX dependently elevated in mice fed the zeaxanthin-free diet (Fig. 7B). Total liver cholesterol (Fig. 7C) was not altered dependently on the genotype and diet. Triacylglycerol level (Fig. 7D) of all mutants mice fed the zeaxanthin diet were lower when compared with wt mice. However, this finding was not reproduced in the mice fed the zeaxanthin-free diet. No significant differences between diets and genotypes were found in serum cholesterol (Fig. 7E) and triacylglycerol levels (Fig. 7F).

The *BCO1* and *ISX* genotypes affect xanthophyll homeostasis of the eyes

Since genetic variability in the *BCO1* gene is not only associated with plasma carotenoid levels but also with macular pigment optical density in humans (20,21), we next analyzed whether the *ISX* and *BCO1* genotypes affected ocular carotenoid homeostasis in the BCO2-deficient mouse model. Hence, we performed HPLC

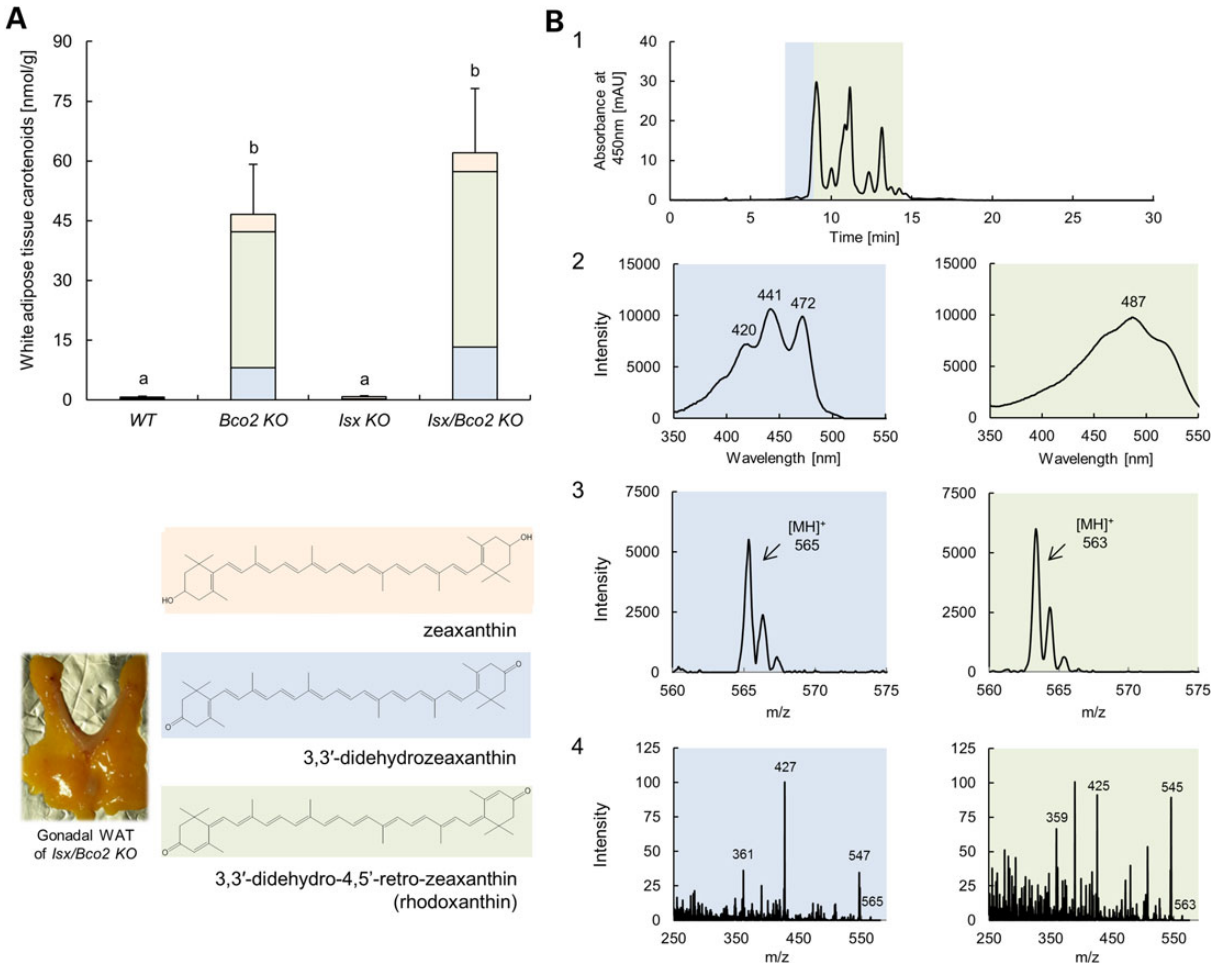

Figure 5. 3,3′-Didehydro-4,5′-retro-zeaxanthin (rhodoxanthin) is the major zeaxanthin metabolites in the WAT. Wild type, *Bco2*$^{-/-}$, *Isx*$^{-/-}$ and *Isx*$^{-/-}$/*Bco2*$^{-/-}$ mice were fed for 10 weeks a zeaxanthin diet based on AIN93G. (**A**) Gonadal WAT levels of zeaxanthin (orange bars), 3,3′-didehydrozeaxanthin (blue bars) and 3,3′-didehydro-4,5′-retro-zeaxanthin (green bars). Values indicate means ± SD from at least five female mice per serum or tissue and genotype. Mean with different letters (a to b) differ significantly. Statistical significance was assessed by one-way ANOVA followed by Scheffe tests using software origin 9, with threshold of significance set at $P < 0.05$. The inset shows the chemical structure of zeaxanthin (orange highlight), 3,3′-didehydrozeaxanthin (blue highlight) and 3,3′-didehydro-4,5′-retro-zeaxanthin (green highlight); and picture of gonadal WAT of *Isx*$^{-/-}$/*Bco2*$^{-/-}$ mouse. (**B**) Identification of zeaxanthin metabolites in gonadal WAT by LC–MS. Panel 1 represents chromatographic separation of zeaxanthin metabolites absorbing at 450 nm. Shoulder of the main peak highlighted in blue corresponds to the known zeaxanthin metabolites 3,3′-didehydrozeaxanthin with characteristic UV/Vis spectra and molecular mass of 564.5 ($m/z = 565.5$ $[MH]^+$ (Panels 2 and 3, blue highlight, respectively). Peaks marked in green correspond to a compound with maximum absorption spectra around 487 nm and molecular mass of 562.3 ($m/z = 563.3$ $[MH]^+$ (Panels 2 and 3, green highlight, respectively) matching molecular characteristics of 3,3′-didehydro-4,5′-retro-zeaxanthin and its geometric isomers. Panel 4 shows averaged MS/MS spectra obtained for 3,3′-didehydrozeaxanthin (blue highlight) and 3,3′-didehydro-4,5′-retro-zeaxanthin (green highlight).

analyses with whole eyes and isolated retinas of *Bco1*$^{-/-}$, *Bco2*$^{-/-}$ and *Bco1*$^{-/-}$/*Bco2*$^{-/-}$ mice supplemented with β-carotene and zeaxanthin together (see above). Xanthophylls were detectable in the eyes of *Bco2*$^{-/-}$ mice and *Bco1*$^{-/-}$/*Bco2*$^{-/-}$ mice but not in *Bco1*$^{-/-}$ mice (Fig. 8A). Notably, most of zeaxanthin existed in the form of its 3,3′-didehydro-derivative in the eyes. Again, the *BCO1* genotype had a strong impact on this accumulation. *Bco1*$^{-/-}$/*Bco2*$^{-/-}$ mice showed 8-fold higher levels of xanthophylls than *Bco2*$^{-/-}$ single mutants. A similar picture emerged when we analyzed the xanthophyll content of the retinas of these mice. Though the overall xanthophyll content was significantly lower when compared with the whole eyes, *Bco1*$^{-/-}$/*Bco2*$^{-/-}$ mice displayed significantly higher levels of this compound in the retina than *Bco2*$^{-/-}$ mice.

To analyze directly whether the *ISX* genotype determines ocular carotenoid levels, we measured ocular xanthophyll levels in *Isx*$^{-/-}$, *Bco2*$^{-/-}$ and *Isx*$^{-/-}$/*Bco2*$^{-/-}$ mice subjected to zeaxanthin feeding. If increased intestinal absorption via SCARB1 accounts for increased ocular xanthophyll levels, *Isx*$^{-/-}$/*Bco2*$^{-/-}$ mice should display significantly higher levels when compared with *Bco2*$^{-/-}$ mice. In fact, HPLC analyses confirmed this assumption by showing 3-fold higher amounts of xanthophyll in the *Isx*$^{-/-}$/*Bco2*$^{-/-}$ compound mutant when compared with *Bco2*$^{-/-}$ single mutant. Again, zeaxanthin existed mainly in the form of its 3,3′-didehydrozeaxanthin derivative (Fig. 8B). Thus, we concluded that augmented intestinal absorption results in significantly increased levels of ocular xanthophyll.

To analyze whether gross xanthophyll accumulation had adverse effects on the mouse eyes, we performed scanning laser ophthalmoscopy (SLO) and optical coherence tomography (OCT) analyses. These analyses revealed that the overall morphology of different retinal layers was not affected by xanthophyll accumulation (Fig. 8C). Additionally, the RPE, choroid and retinal vascularization appeared normal in these mice.

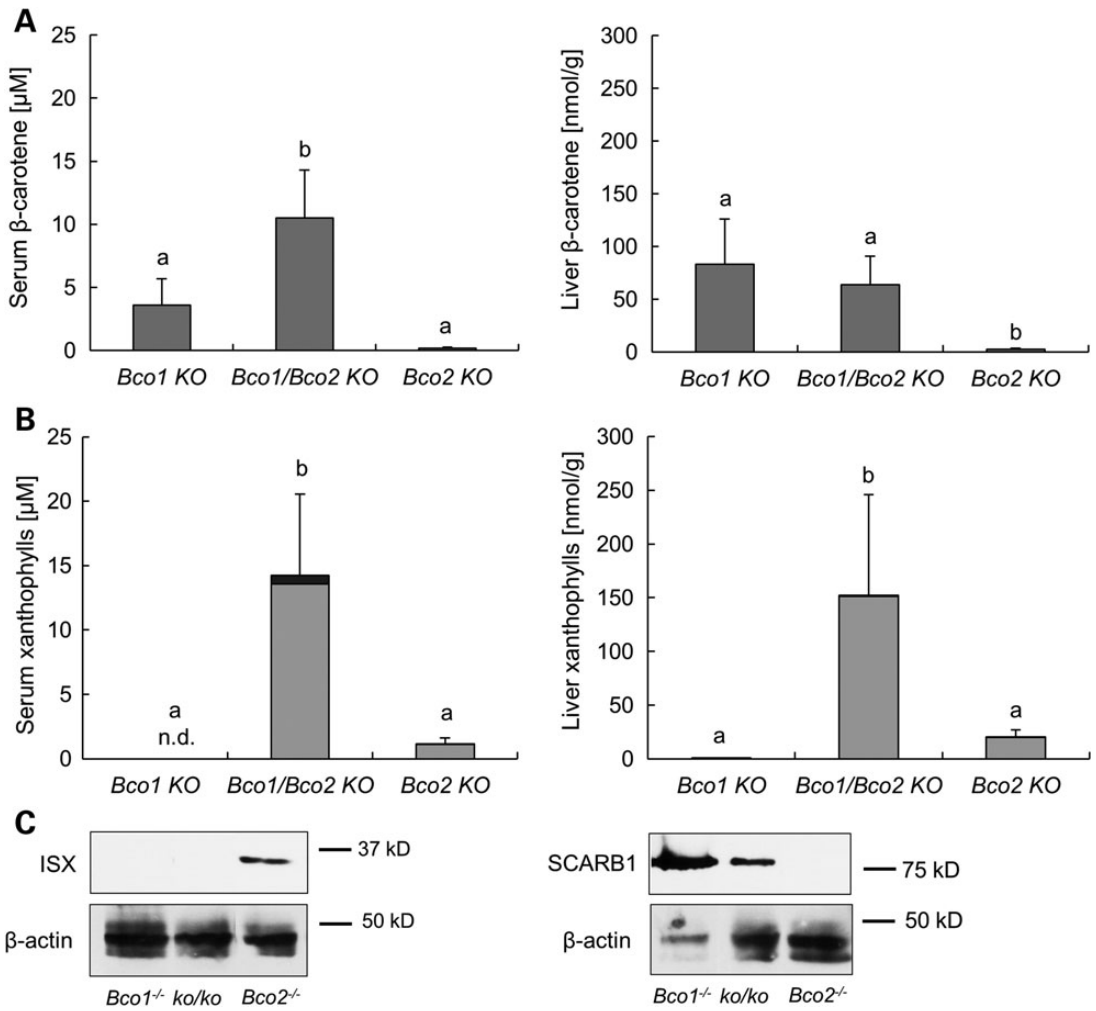

Figure 6. BCO1 controls xanthophyll absorption. *Bco1*$^{-/-}$, *Bco2*$^{-/-}$ and *Bco1*$^{-/-}$/*Bco2*$^{-/-}$ mice were fed for 10 weeks a zeaxanthin and β-carotene mixed diet, with the vitamin A source solely from β-carotene. (**A**) Serum (left) and hepatic (right) levels of β-carotene. (**B**) Serum (left) and hepatic (right) levels of 3,3′-didehydrozeaxanthin (gray bars) and zeaxanthin (black bars). Values indicate means ± SD from at least five female mice per serum or tissue and genotype. Mean with different letters (a to b) differ significantly. Statistical significance was assessed by one-way ANOVA followed by Scheffe tests using software origin 9, with threshold of significance set at $P < 0.05$. (**C**) Total protein of these different mice genotype was obtained from jejunum and subjected to immunoblot analysis and subsequently probed with ISX (left) and SCARB1 (right) antibodies. β-actin served as a loading control.

Furthermore, xanthophyll accumulation did not disturb ocular retinoid metabolism and the visual cycle as indicated by a normal retinoid composition of the eyes (Fig. 8D).

Discussion

Oxidative stress has been related to chronic disease including cardiovascular disease, cancer and ocular diseases. Dietary antioxidants such as carotenoids and tocopherols can scavenge free radicals and reactive oxygen species thereby delaying disease onset and progression. Surprisingly, the plasma and tissue concentration of these lipids are highly variable between individuals and only weakly correlate with dietary intake. Genome-wide and candidate gene association studies in various large cohorts indicate that genetic polymorphism in the *BCO1* gene affects plasma and tissue levels of carotenoids. Here, we showed by genetic dissection in mouse models that fat-soluble vitamin and carotenoid absorption is a regulated process and that intestinal BCO1 activity is a critical control element in this regulation. Thus, our studies provide a molecular framework for the controversial relationship between genetics and fat-soluble vitamin status in the human population.

BCO1 is a key component of a regulatory network that controls fat-soluble vitamin and carotenoid absorption

Previously, we provided evidence that intestinal vitamin A production is under negative feedback regulation. In this process, the homeobox transcription factor ISX suppresses the intestinal expression of the vitamin A forming enzyme BCO1 through a cross-talk between retinoid and ISX signaling (34,35) (Fig. 1). ISX is a homeobox transcription factor that is expressed in the epithelia of the intestine already early in gut development (36,38). In transcriptome analysis, the scavenger receptor SCARB1 also was identified as a target gene of ISX signaling (36,38). However, it has been not demonstrated that ISX controls intestinal SCARB1 activity. We here showed that SCARB1 protein levels are elevated in the intestine of *Isx*$^{-/-}$ mice. We further provide evidence that the interaction between ISX and the *SCARB1* gene is direct as indicated by EMSA experiments (Fig. 3). The identified ISX-binding site upstream of

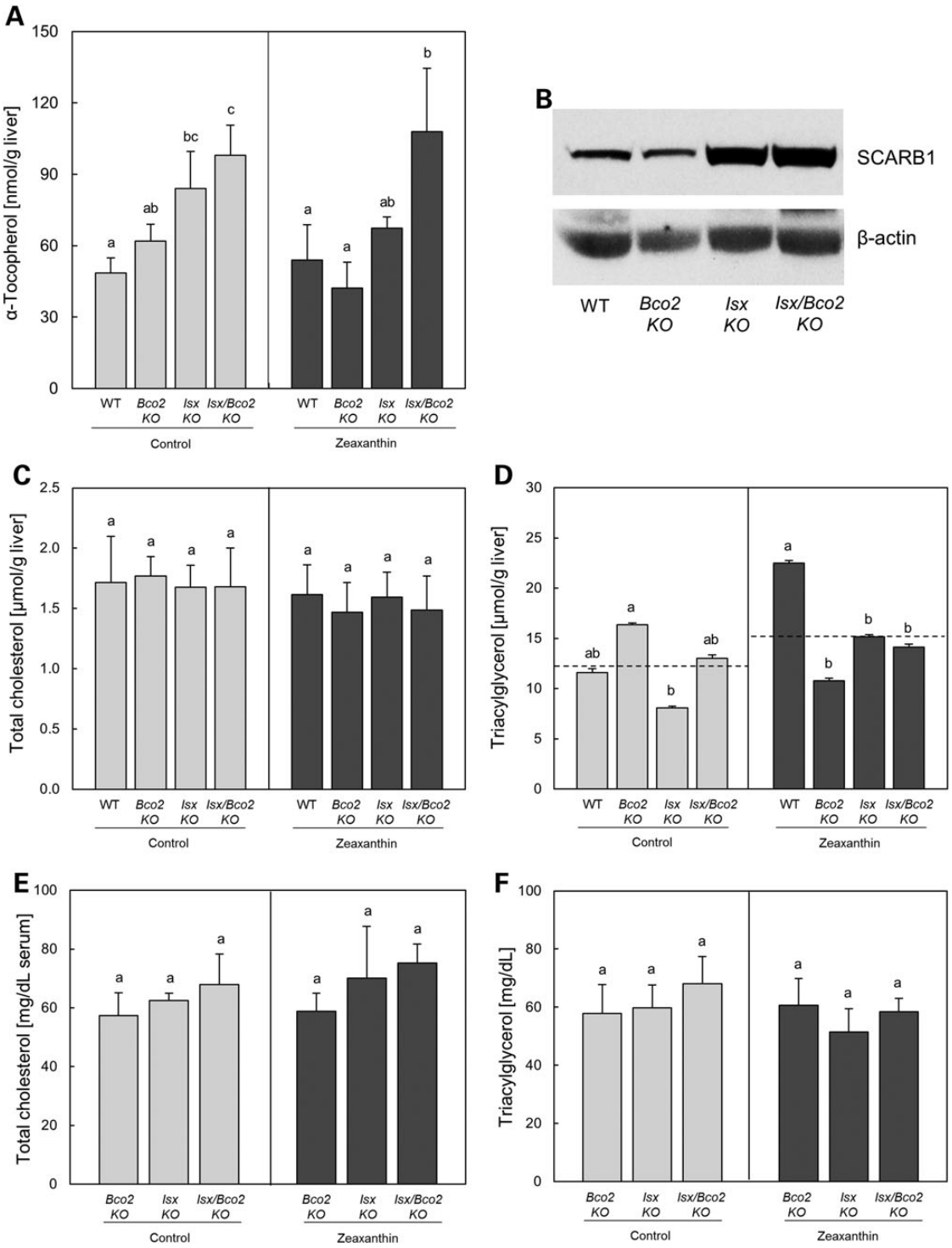

Figure 7. *ISX* genotype affects fat-soluble vitamin status. Wild type, $Bco2^{-/-}$, $Isx^{-/-}$ and $Isx^{-/-}/Bco2^{-/-}$ mice were fed for 10 weeks a zeaxanthin diet (dark bar) or control diet (light bar) based on AIN93G. Hepatic levels of α-tocopherol (**A**), total protein of different mice genotype under zeaxanthin-free diets was obtained from jejunum and subjected to immunoblot analysis and subsequently probed with SCARB1 antibodies (**B**), hepatic total cholesterol (**C**) and triacylglycerol (**D**), and serum levels of cholesterol (**E**) and triacylglycerol (**F**). Values indicate means ± SD from at least three female mice per tissue and genotype or five female mice per serum and genotype. Mean with different letters (a to c) differ significantly. Statistical significance was assessed by one-way ANOVA followed by Scheffe tests using software origin 9, with threshold of significance set at $P < 0.05$.

the *SCARB1* gene shared sequence identity with identified binding site upstream of the *BCO1* gene and competed for ISX binding in EMSA experiments. Consistent with its role as transcriptional repressor, binding of ISX to this site was sufficient to suppress the expression of a reporter gene in human Caco-2 cells (35), indicating that the binding site is part of a repressor element.

SCARB1 was first described as a critical component of cholesterol transport from circulating high-density lipoproteins (53).

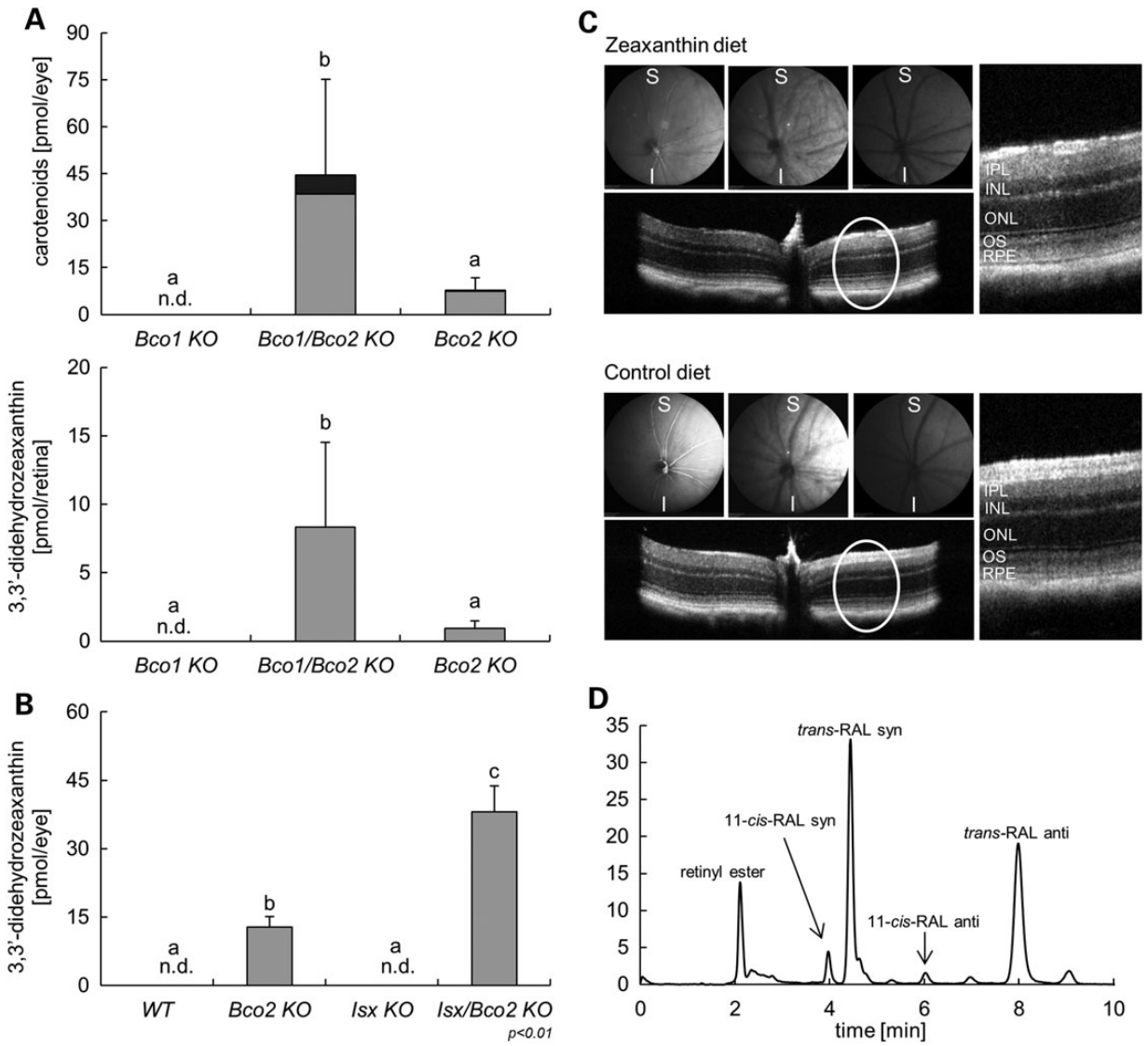

Figure 8. *BCO1* and *ISX* genotypes affect xanthophyll homeostasis of the eyes. (**A**) Whole eye (top) and retina (bottom) levels of 3,3′-didehydrozeaxanthin (gray bars) and parent zeaxanthin (black bars) of $Bco1^{-/-}$, $Bco2^{-/-}$ and $Bco1^{-/-}/Bco2^{-/-}$ mice fed for 10 weeks a zeaxanthin and β-carotene mixed diet, with vitamin A source solely come from β-carotene. (**B**) Whole eye levels of 3,3′-didehydrozeaxanthin (gray bars) of wt, $Bco2^{-/-}$, $Isx^{-/-}$ and $Isx^{-/-}/Bco2^{-/-}$ mice fed for 10 weeks a zeaxanthin diet based on AIN93G. Values indicate means ± SD from at least five female mice per eye or retina and genotype. Mean with different letters (a to c) differ significantly. Statistical significance was assessed by one-way ANOVA followed by Scheffe tests using software origin 9, with threshold of significance set at $P < 0.05$. (**C**) *In vivo* imaging of $Isx^{-/-}/Bco2^{-/-}$ mice fed for 10 weeks with either a zeaxanthin (top) or control diet (bottom) was performed by SLO and high-definition spectral domain optical coherent tomography (SD-OCT). No disruption of the morphology of different retinal layers (circle and enlarged) by SD-OCT and images by SLO with xanthophyll accumulation in the eye of $Isx^{-/-}/Bco2^{-/-}$ mice fed zeaxanthin diet. S, superior; I, inferior; IPL, inner plexiform layer; INL, inner nuclear layer; ONL, outer nuclear layer; OS, outer segment; RPE, retinal pigmented epithelium (**D**) HPLC profile at 360 nm of eye extracts from $Isx^{-/-}/Bco2^{-/-}$ mice fed zeaxanthin diet.

Over the years, experimental evidence accumulated that SCARB1 also mediates cellular uptake of other isoprenoid compounds including tocopherols and carotenoids (reviewed in 39). Here, we performed a genetic approach to show that SCARB1 deficiency reduced xanthophyll absorption in the intestine (Fig. 2). Conversely, we demonstrated that increased intestinal SCARB1 protein levels in ISX deficiency were correlated with increased xanthophyll absorption levels of mice (Fig. 4). Our studies further showed that ISX controlled xanthophyll absorption whereas BCO2 controlled xanthophyll levels in tissues. Accordingly, the loss of both components led to enhanced xanthophyll absorption and tissue accumulation as seen in the double-knockout mice (Figs 4 and 5). We identified BCO1 as key component for this regulation. For these experiments, we employed mice deficient for BCO1 and BCO2 or either carotenoid oxygenase (Fig. 6). We subjected these mice to a diet providing zeaxanthin and β-carotene together. Analysis in different genotypes revealed that β-carotene and zeaxanthin accumulated in $Bco1^{-/-}$ and $Bco2^{-/-}$ mice, respectively. The *BCO1* genotype had a tremendous effect on zeaxanthin accumulation as seen in the double-knockout mice. These mice displayed significantly higher levels of xanthophyll in tissues than $Bco2^{-/-}$ single-knockout mice (Fig. 6). The impact of BCO1 on zeaxanthin tissue levels is in accordance with β-carotene-dependent retinoid signaling that controls ISX expression in the intestine. In fact, ISX protein was present in the intestine of $Bco2^{-/-}$ mice but was below detection levels

in *Bco1*$^{-/-}$ mutants and double mutants that cannot convert β-carotene to retinoids (Fig. 6). Again, SCARB1 protein levels were dependent on ISX and showed the opposite pattern of expression. In contrast to the effect of BCO1 on zeaxanthin metabolism, BCO2 had no effect on β-carotene metabolism, thus confirming previous studies of our laboratory (51). Thus, our studies in mouse models indicated that the interaction between BCO1 and xanthophyll metabolism is indirect and relied on the role of retinoids in the control of intestinal ISX activity which controls *SCARB1* expression levels and carotenoid absorption.

Our study also revealed that the ISX-dependent regulation of intestinal SCARB1 activity affected tocopherol levels in tissues of mice (Fig. 7). However, the difference between hepatic α-tocopherol levels in ISX deficient and sufficient animals was not as pronounced as for carotenoids. The milder effect of ISX deficiency on tocopherol levels might be explained by additional proteins that contribute to the intestinal absorption of this vitamin. These proteins may include ABC transporters and Nieman Pick C1-like 1 protein (54). In contrast to tocopherols and carotenoids, cholesterol levels in plasma and liver were not affected by the *ISX* genotype (Fig. 7). This observation confirmed a previous study that reports that ISX deficiency has no major impact on cholesterol homeostasis of mice (36).

Individual genetics can affect the response to dietary carotenoids

In humans, carotenoid and tocopherol plasma and tissue levels are variable and weakly correlate with dietary intake (19,55–57). The identification of molecular components of the path for fat-soluble vitamin and carotenoid absorption and metabolism revealed that genetics contributes to this variability (20–23). Common genetic polymorphisms in identified genes are associated with carotenoid and tocopherol plasma and tissue levels. The ISX-dependent regulation of carotenoid absorption and metabolism adds an additional layer to the complexity of this phenomenon. The relevance of this regulation for human physiology has just been indicated by the finding that genetic polymorphism in *ISX* gene affects the bioavailability of the carotenoid lutein (55). In previous studies, the *BCO1* and *SCARB1* genes already have been associated with plasma levels of xanthophylls and macular pigment optical density (20–23). Our genetic analyses in mice provide a mechanistic explanation how intestinal BCO1 activity can affect xanthophyll plasma and tissue levels though these compounds are no substrates for the enzyme. As we showed here, BCO1-dependent retinoid production from β-carotene controlled xanthophyll absorption via ISX. This control did not only affect plasma but also ocular levels of carotenoids in the BCO2-deficient mouse model. Ocular levels of zeaxanthin and its 3-oxo-metabolites were 8-fold higher in *Bco1*$^{-/-}$/*Bco2*$^{-/-}$ compound mutants as compared with *Bco2*$^{-/-}$ single mutants (Fig. 8). Consistently, ocular xanthophyll levels were also higher in *Isx*$^{-/-}$/*Bco2*$^{-/-}$ compound mutant mice when compared with *Bco2*$^{-/-}$ mice (Fig. 8). Notably, genetic polymorphisms in the *BCO1* gene also have been associated with a higher risk of the blinding disease AMD (22), thus adding to the emerging body of evidence for a retinal protective role of carotenoids. However, this role of carotenoids is rather an assumption than an experimentally proven fact. Testing this hypothesis was hampered by the lack of small mammalian models with a carotenoid-rich retina. The generation of mouse models with a carotenoid-rich retina will allow us to evaluate the retinal protective role of these pigments in an animal model with striking similarity to humans in anatomy, physiology and genetics. Though there are clear limitations such as absence of a cone-rich *fovea centralis*, these mouse models will allow exploring the role of carotenoids in ocular disease states related to oxidative stress and inflammation.

In conclusion, we provide evidence in mice that the homeostasis of carotenoids and fat-soluble vitamins A and E is subject to regulation at the level of intestinal absorption and identified ISX, SCARB1 and BCO1 as key components for this process. The existence of common genetic polymorphisms in these genes and their association with plasma and tissue levels of these compounds in humans demonstrate the clinical significance of our findings. As human longevity and nutritional technology increase, an improved understanding of the regulatory principles governing the homeostasis of 'tissue protective' carotenoids and fat-soluble vitamins will become a necessity. This knowledge will help to appraise the consequences of common genetic variability and eventually lead to personalized recommendations for nutrition/supplementation.

Materials and Methods

Animals, husbandry and experimental diets

Animal procedures and experiments were approved by the Case Western Reserve University Animal Care Committee and conformed to recommendations of both the American Veterinary Medical Association Panel on Euthanasia and the ARVO Statement for the Use of Animals in Ophthalmic and Vision Research. Animal experiments were carried out using 5-week-old female *Bco2*$^{-/-}$, *Isx*$^{-/-}$, *Isx*$^{-/-}$/*Bco2*$^{-/-}$ and wt control mice. All mice were on a C57/BL6;129Sv mixed genetic background. The generation of *Bco2*$^{-/-}$ and *Isx*$^{-/-}$ mice has been previously described (36,40). Double-knockout *Isx*$^{-/-}$/*Bco2*$^{-/-}$ mice were established by conventional cross-breeding. In all experiments, mice were maintained at 24°C in a 12- to 12-h light–dark cycle and had free access to food and water. During the breeding and weaning periods (up to 5 weeks of age), mice were maintained on breeder chow containing ~29 000 IU vitamin A/kg diet (Prolab RMH 3000; LabDiet, St. Louis, MO, USA). After 5 weeks of age, mice were fed experimental diet based on AIN93G formulation containing 4000 IU vitamin A/kg diet with added zeaxanthin or placebo beadlets as the control diet for 10 weeks. The zeaxanthin diet contained 50 mg zeaxanthin/kg diet. This diet was prepared by Research Diets, Inc. (New Brunswick, NJ, USA) by incorporating a water-soluble formulation of zeaxanthin or placebo beadlets (DSM Ltd., Sisseln, Switzerland). After 10 weeks of dietary intervention, mice were fasted overnight and anesthetized by intraperitoneal injection of a mixture containing ketamine 15 mg, Xylazine 3 mg, Acepromazine 0.5 mg and sterile water or saline, with a dose of 0.2 ml/25 g of mouse. Blood was drawn directly from the heart by cardiac puncture under deep anesthesia. Mice were then perfused with 20 ml of PBS (137 mM NaCl, 2.7 mM KCl, 4.3 mM Na_2HPO_4, 1.4 mM KH_2PO_4, pH 7.3) and killed by cervical dislocation for further tissue collection. To provide *in vivo* evidence that SCARB1 facilitates the uptake of xanthophylls, we produced double-knockout *Scarb1*$^{-/-}$/*Bco2*$^{-/-}$ mice by conventional cross-breeding. *Scarb1*$^{-/-}$ mice (B6;129S2-*Scarb1*$^{tm1Kri/J}$) were obtained from Jackson laboratory (stock number 003379). The dietary intervention was performed as described earlier with an experimental diet containing zeaxanthin (150 mg/kg diet) with no source for preformed vitamin A. Sex- and age-matched *Bco2*$^{-/-}$ mice were used as controls. To confirm that BCO1 impacts xanthophyll absorption, we carried out a dietary intervention study. We used 5-week-old female *Bco1*$^{-/-}$, *Bco2*$^{-/-}$ and *Bco1*$^{-/-}$/*Bco2*$^{-/-}$ mice with a C56/BL6;129Sv

mixed genetic background. The generation of *Bco1*$^{-/-}$, *Bco2*$^{-/-}$ and *Bco1*$^{-/-}$/*Bco2*$^{-/-}$ has been previously described (40,47,51). All other conditions were the same as per above, except that mice were fed an experimental diet containing a mixture of β-carotene and zeaxanthin (25 and 75 mg/kg diet for each carotenoid, respectively) for 10 weeks. The diet contained no other source of vitamin A except for β-carotene.

Immunoblotting

Immunoblot analysis was used to determine SCARB1 and ISX protein levels of the small intestine (jejunum) from each mouse. Tissues samples were homogenized in M-PER mammalian protein extraction reagent (Thermo Scientific, Marietta, OH, USA) following the manufacturer's instructions. Total protein concentration in the tissue extract was determined using the Bio-Rad protein assay. Based on the method of Bradford (Bio-Rad Laboratories, Hercules, CA, USA), 25 μg of total protein was loaded per lane and separated by SDS–PAGE and then electroblotted onto PVDF membranes (Bio-Rad Laboratories). Membranes were blocked with fat-free milk powder (5% w/v) dissolved in Tris-buffered saline (15 mM NaCl and 10 mM Tris–HCl, pH 7.5) containing 0.05% Tween-20 (TBS-T), washed and incubated overnight at 4°C with the goat SCARB1 antibody (NB400-131 from Novus Biologicals, LLC., Littleton, CO, USA) or the rabbit ISX antibody (sc-86151 from Santa Cruz Biotechnology) with a 1 : 1000 dilution followed by horseradish peroxidase-conjugated anti-goat IgG (172–1034) or anti-rabbit IgG (170–6515) (Bio-Rad Laboratories), respectively, at a dilution of 1 : 5000 and then visualized using an ECL chemiluminescent detection kit (K-12042-D10 from Advansta, Inc., Menlo Park, CA, USA). β-Actin antibody (Santa Cruz Biotechnology, Inc., Dallas, TX, USA) at a dilution of 1 : 10 000 served as a loading control.

HPLC separation of carotenoids

Carotenoids were extracted from tissues of mice ($n = 5$ per genotype and diet) under a dim red safety light (600 nm) and quantified by HPLC. Briefly, 75 mg of liver or 100 μl of serum were extracted using 300 μl of methanol, 600 μl of acetone, 300 μl of diethyl ether and 400 μl of hexane. The organic phase was removed and the extraction was repeated with additional 500 μl of hexanes. After centrifugation, organic layers were collected, pooled and dried in a SpeedVac (Eppendorft, Hamburg, Germany) at 30°C and re-dissolved in HPLC mobile-phase solvent. For saponification, gonadal WATs were homogenized in 200 μl of 30% KOH in water then incubated with 100 μl of 12% pyrogallol (Sigma) in ethanol and 1 ml ethanol for 1 h at 60°C. After saponification, 2 ml of ethanol and 2 ml of H_2O were added and samples were extracted twice with 3 ml of diethyl ether/hexane (2 : 1, stabilized with 1% ethanol). The organic layers were collected, pooled and evaporated in a SpeedVac (Eppendorf, Hauppauge, NY, USA) until near dry. The second extraction solution was then added to the near dry solution. The extraction solution was composed of 200 μl of water, 200 μl of methanol, 400 μl of acetone, 250 μl of diethyl ether and 400 μl of hexane. The organic phase was then removed, and the extraction was repeated with 500 μl of hexanes. After centrifugation, organic layers were collected, pooled and dried in a SpeedVac (Eppendorf) at 30°C and re-dissolved in HPLC mobile-phase solvent. The HPLC analysis was carried out with an Agilent 1260 Infinity Quaternary HPLC system (Santa Clara, CA, USA) equipped with a pump (G1312C) with an integrated degasser (G1322A), a thermostated column compartment (G1316A), an autosampler (G1329B), a diode-array detector (G1315D) and online analysis software (Chemstation). The analyses were carried out at 25°C using a normal-phase Zorbax Sil (5 μm, 4.6 × 150 mm) column (Agilent Technologies, Santa Clara, CA, USA) protected with a guard column with the same stationary phase. For xanthophyll separation, 30% of ethyl acetate was mixed with 70% hexane. For β-carotene separation from the tissues of mixed-diet mice, a step gradient of 1% ethyl acetate in hexane over 5 min followed by 10 min with 10% ethyl acetate in hexane and then 15 min with 40% ethyl acetate in hexane was used. In both cases, the flow rate was 1.4 ml/min. For molar quantification of carotenoids by UV/Vis absorbance, the HPLC was scaled with zeaxanthin and β-carotene standards.

Tandem mass spectrometry (MS/MS)

Carotenoids and their metabolites were extracted and separated on an 1100 Agilent HPLC series equipped with diode-array detector and Zorbax Sil (5 μm, 4.6 × 150 mm) column (Agilent), equilibrated with 30% ethyl acetate in hexane as described earlier. The elute at a flow rate of 1.4 ml/min was directed into an LXQ linear ion trap mass spectrometer (Thermo Scientific, Waltham, MA, USA) through atmospheric pressure chemical ionization source working in the positive mode. To ensure optimal sensitivity, the instrument was tuned for zeaxanthin.

HPLC separation of α-tocopherol

HPLC analyses for *α-tocopherol* were carried out with the same system as described earlier except that the mobile phase was hexane: 2-propanol (99.2 : 0.8, v/v). The flow rate was 1.0 ml/min. For the quantification of molar amounts, the HPLC system was scaled with (±)-*α-tocopherol*. (±)-*α-tocopherol* (T3251) was obtained from Sigma–Aldrich.

ISX protein extracts for DNA-binding assays

ISX protein was obtained by the transformation of *Escherichia Coli* BL21 cells with a bacterial expression vector containing the full-length mouse ISX cDNA (pTrcHis2-WT-ISX) previously described (35). Expression of ISX protein in different supernatant and pellet fractions were determined by immunoblot analysis using an anti-His antibody (Qiagen, Inc., Valencia, CA, USA). In subsequent EMSAs, ISX protein in the supernatant fractions was used.

Cloning of the ISX-binding site upstream of the *SCARB1* gene

The 5′-upstream region of the mouse *SCARB1* gene (−6.4 to −4.5 kb, relevant to the SCARB1 ATG start site) was subdivided into three overlapping DNA fragments (~540–730 bp in length). Each fragment was PCR-amplified with genomic DNA isolated from mouse intestine as template and oligonucleotide primer pairs as follows: for *SCARB1* fragment-1 (635 bp): *SCARB1frag*1-1-Fwd 5′ GCAGTGTAACCTCTCCTCTGT 3′ and *SCARB1*-frag-1-Rev 5′ TAAAGACCCAAGTCCTTGCT GT 3′; for *Scarb*1 fragment-2 (730 bp): *SCARB1*-frag-2-Fwd 5′ GCCCATTGGCTTCCTGCTGA GT 3′ and *SCARB1*-frag-2-Rev 5′ ACCCTGGTGTGTCTGAAGACAGC 3′; for *SCARB1*-fragment-3 (539 bp): *SCARB1*-frag-3-Fwd 5′ GCATGG TGGCACACACCTTGAA 3′ and *SCARB1*-frag-3-Rev 5′ AGAAACTGC TGAGGGCTGAGC 3′ by using PCR conditions as described previously (35,58). *SCARB1*-fragment 2 (nucleotides −5760 to −5030) contained a putative ISX-binding site, with high sequence identity to the ISX-binding site upstream if the *BCO1* gene (35). *SCARB1* promoter fragments 1 and 3 (lacking the consensus ISX-binding sequences) flanked the *SCARB1*-fragment 2 and served as controls in EMSA experiments. The individual *SCARB1*

fragments were cloned into the pTrcHis2 TOPO TA vector according to the manufacturer's protocols (Invitrogen, Carlsbad, CA, USA). Appropriate construction and cloning of *SCARB1* promoter fragments were confirmed by direct sequencing of both nucleotide strands.

Biotin 3′ end DNA labeling of individual *SCARB1* promoter fragments

The three individual *SCARB1* fragments cloned into the pTrcHis2 TOPO TA vector were excised with *Nco*I and *Eco*RI restriction enzymes (New England BioLabs, Inc., Ipswich, MA, USA). Restricted *SCARB1* fragments were gel-purified (Qiagen, Inc.) and eluted in Tris–EDTA (TE) buffer. Following purification, individual *SCARB1* DNA fragments were labeled using the non-isotopic Biotin 3′ End DNA labeling kit as outlined by the manufacturer (Pierce/Thermo Scientific, Rockford, IL, USA).

Electrophoresis mobility shift assays

Electrophoresis mobility shift assays were carried out according to published procedures (35,59). Briefly, biotin-labeled *SCARB1* fragments 1, 2 and 3) were incubated for 10 min at room temperature (RT) with crude ISX protein extract from BL21 cells in EMSA buffer containing 10 mM Tris–HCl, pH 7.5, 50 mM NaCl, 3 mM $MgC1_2$, 1 mM EDTA and 10% glycerol. 6% non-denaturing polyacrylamide gels (PAGE) in 0.5× TBE buffer were pre-electrophoresed for 30 min at RT. Protein–DNA complexes were then separated from unbound DNA on these 6% PAGE gels for 45–60 min at RT. The PAGE gels containing protein–DNA complexes were then transferred on to positively-charged nylon membranes (Biodyne B membranes, Thermo Scientific) using the Bio-Rad mini-gel transfer apparatus in 0.5× TBE buffer. Nylon membranes were incubated with streptavidin–HRP and chemiluminescent substrate reagents (Pierce ECL from Thermo Scientific) followed by exposure and visualization complexes by X-ray film exposure. To prevent nonspecific binding of proteins to biotin-labeled DNA fragments, the synthetic heteropolymer poly dI-dC was added at a concentration of 2 μg/μl per reaction. To confirm that the observed protein–DNA complexes resulted from specific binding, a 100-fold molar excess of the corresponding unlabeled *SCARB1* fragments was added to compete with nonspecific protein–DNA binding. All EMSA images in relevant figures are representative of at least two independent experiments.

SD-OCT and fundus acquisition

With pupils fully dilated with 1% tropicamide (Falcon Pharmaceuticals, Fort Worth, TX, USA), mice were anesthetized with an intraperitoneal injection a mixture containing ketamine 15 mg, Xylazine 3 mg, Acepromazine 0.5 mg and sterile water or saline, with a dose of 0.2 ml/25 g of mouse. Whiskers were trimmed carefully to avoid image artifacts. OCT images were acquired with linear B-scan mode by employing ultra-high-resolution SD-OCT (Bioptigen).

Mouse fundus imaging was then performed with a cSLO (SpectralisHRA2, Heidelberg Engineering, Heidelberg, Germany) with a 55° lens. The near infrared reflectance image (IR mode, 820 nm laser) was used to align the fundus camera relative to the pupil to obtain an evenly illuminated fundus image.

Statistical analyses

Results are presented as means ± SD, and the number of experiments is indicated in the figure legends. The analysis technique was not sensitive enough to detect data point denoted 'n.d.' (not detected) so the value of these points was forced to zero. Statistical significance was assessed by one-way analysis of variance (ANOVA) followed by Scheffe test tests using software origin 9 (OriginLab Corporation, Northampton, MA, USA), with threshold of significance set at $P < 0.05$.

Conflict of Interest statement. None declared.

Funding

This work was supported by grants from the National Eye Institute (RO1EY019641 and RO1EY020551) of the U.S. National Institute of Health and by startup funds of Case Western Reserve University.

References

1. Demmig-Adams, B. and Adams, W.W. 3rd. (2002) Antioxidants in photosynthesis and human nutrition. *Science*, **298**, 2149–2153.
2. Hammond, B.R. Jr., Johnson, E.J., Russell, R.M., Krinsky, N.I., Yeum, K.J., Edwards, R.B. and Snodderly, D.M. (1997) Dietary modification of human macular pigment density. *Invest. Ophthalmol. Vis. Sci.*, **38**, 1795–1801.
3. Snodderly, D.M. (1995) Evidence for protection against age-related macular degeneration by carotenoids and antioxidant vitamins. *Am. J. Clin. Nutr.*, **62**, 1448S–1461S.
4. Snodderly, D.M., Handelman, G.J. and Adler, A.J. (1991) Distribution of individual macular pigment carotenoids in central retina of macaque and squirrel monkeys. *Invest. Ophthalmol. Vis. Sci.*, **32**, 268–279.
5. Bone, R.A., Landrum, J.T. and Tarsis, S.L. (1985) Preliminary identification of the human macular pigment. *Vision Res.*, **25**, 1531–1535.
6. SanGiovanni, J.P. and Neuringer, M. (2012) The putative role of lutein and zeaxanthin as protective agents against age-related macular degeneration: promise of molecular genetics for guiding mechanistic and translational research in the field. *Am. J. Clin. Nutr.*, **96**, 1223S–1233S.
7. Hammond, B.R. Jr. and Fletcher, L.M. (2012) Influence of the dietary carotenoids lutein and zeaxanthin on visual performance: application to baseball. *Am. J. Clin. Nutr.*, **96**, 1207S–1213S.
8. von Lintig, J. (2010) Colors with functions: elucidating the biochemical and molecular basis of carotenoid metabolism. *Annu. Rev. Nutr.*, **30**, 35–56.
9. Eroglu, A. and Harrison, E.H. (2013) Carotenoid metabolism in mammals including man:formation, occurrence & function of apocarotenoids. *J. Lipid Res.*, **54**, 1719–1730.
10. Krinsky, N.I., Landrum, J.T. and Bone, R.A. (2003) Biologic mechanisms of the protective role of lutein and zeaxanthin in the eye. *Annu. Rev. Nutr.*, **23**, 171–201.
11. Beatty, S., Boulton, M., Henson, D., Koh, H.H. and Murray, I.J. (1999) Macular pigment and age related macular degeneration. *Br. J. Ophthalmol.*, **83**, 867–877.
12. Johnson, E.J. (2012) A possible role for lutein and zeaxanthin in cognitive function in the elderly. *Am. J. Clin. Nutr.*, **96**, 1161S–1165S.
13. Semba, R.D., Lauretani, F. and Ferrucci, L. (2007) Carotenoids as protection against sarcopenia in older adults. *Arch. Biochem. Biophys.*, **458**, 141–145.
14. Bone, R.A., Landrum, J.T., Mayne, S.T., Gomez, C.M., Tibor, S.E. and Twaroska, E.E. (2001) Macular pigment in donor eyes with

and without AMD: a case-control study. *Invest. Ophthalmol. Vis. Sci.*, **42**, 235–240.
15. Chew, E.Y., Clemons, T.E., Sangiovanni, J.P., Danis, R.P., Ferris, F.L. 3rd, Elman, M.J., Antoszyk, A.N., Ruby, A.J., Orth, D., Bressler, S.B. *et al.* (2014) Secondary analyses of the effects of lutein/zeaxanthin on age-related macular degeneration progression: AREDS2 report No. 3. *JAMA Ophthalmol.*, **132**, 142–149.
16. Chew, E.Y., SanGiovanni, J.P., Ferris, F.L., Wong, W.T., Agron, E., Clemons, T.E., Sperduto, R., Danis, R., Chandra, S.R., Blodi, B.A. *et al.* (2013) Lutein/zeaxanthin for the treatment of age-related cataract: AREDS2 randomized trial report no. 4. *JAMA Ophthalmol.*, **131**, 843–850.
17. Bhosale, P., Zhao da, Y. and Bernstein, P.S. (2007) HPLC measurement of ocular carotenoid levels in human donor eyes in the lutein supplementation era. *Invest. Ophthalmol. Vis. Sci.*, **48**, 543–549.
18. Mares, J.A., LaRowe, T.L., Snodderly, D.M., Moeller, S.M., Gruber, M.J., Klein, M.L., Wooten, B.R., Johnson, E.J. and Chappell, R.J. (2006) Predictors of optical density of lutein and zeaxanthin in retinas of older women in the Carotenoids in Age-Related Eye Disease Study, an ancillary study of the Women's Health Initiative. *Am. J. Clin. Nutr.*, **84**, 1107–1122.
19. Borel, P., Grolier, P., Mekki, N., Boirie, Y., Rochette, Y., Le Roy, B., Alexandre-Gouabau, M.C., Lairon, D. and Azais-Braesco, V. (1998) Low and high responders to pharmacological doses of beta-carotene: proportion in the population, mechanisms involved and consequences on beta-carotene metabolism. *J. Lipid Res.*, **39**, 2250–2260.
20. Meyers, K.J., Johnson, E.J., Bernstein, P.S., Iyengar, S.K., Engelman, C.D., Karki, C.K., Liu, Z., Igo, R.P. Jr., Truitt, B., Klein, M.L. *et al.* (2013) Genetic determinants of macular pigments in women of the Carotenoids in Age-Related Eye Disease Study. *Invest. Ophthalmol. Vis. Sci.*, **54**, 2333–2345.
21. Borel, P., de Edelenyi, F.S., Vincent-Baudry, S., Malezet-Desmoulin, C., Margotat, A., Lyan, B., Gorrand, J.M., Meunier, N., Drouault-Holowacz, S. and Bieuvelet, S. (2011) Genetic variants in BCMO1 and CD36 are associated with plasma lutein concentrations and macular pigment optical density in humans. *Ann. Med.*, **43**, 47–59.
22. Meyers, K.J., Mares, J.A., Igo, R.P. Jr., Truitt, B., Liu, Z., Millen, A.E., Klein, M., Johnson, E.J., Engelman, C.D., Karki, C.K. *et al.* (2014) Genetic evidence for role of carotenoids in age-related macular degeneration in the Carotenoids in Age-Related Eye Disease Study (CAREDS). *Invest. Ophthalmol. Vis. Sci.*, **55**, 587–599.
23. Ferrucci, L., Perry, J.R., Matteini, A., Perola, M., Tanaka, T., Silander, K., Rice, N., Melzer, D., Murray, A., Cluett, C. *et al.* (2009) Common variation in the beta-carotene 15,15′-monooxygenase 1 gene affects circulating levels of carotenoids: a genome-wide association study. *Am. J. Hum. Genet.*, **84**, 123–133.
24. Hendrickson, S.J., Hazra, A., Chen, C., Eliassen, A.H., Kraft, P., Rosner, B.A. and Willett, W.C. (2012) beta-Carotene 15,15′-monooxygenase 1 single nucleotide polymorphisms in relation to plasma carotenoid and retinol concentrations in women of European descent. *Am. J. Clin. Nutr.*, **96**, 1379–1389.
25. Wyss, A., Wirtz, G.M., Woggon, W.D., Brugger, R., Wyss, M., Friedlein, A., Riss, G., Bachmann, H. and Hunziker, W. (2001) Expression pattern and localization of beta,beta-carotene 15,15′-dioxygenase in different tissues. *Biochem. J.*, **354**, 521–529.
26. Lindqvist, A. and Andersson, S. (2002) Biochemical properties of purified recombinant human beta-carotene 15,15′-monooxygenase. *J. Biol. Chem.*, **277**, 23942–23948.
27. Dela Sena, C., Riedl, K.M., Narayanasamy, S., Curley, R.W. Jr., Schwartz, S.J. and Harrison, E.H. (2014) The human enzyme that converts dietary provitamin a carotenoids to vitamin a is a dioxygenase. *J. Biol. Chem.*, **289**, 13661–13666.
28. von Lintig, J. and Vogt, K. (2000) Filling the gap in vitamin A research. Molecular identification of an enzyme cleaving beta-carotene to retinal. *J. Biol. Chem.*, **275**, 11915–11920.
29. von Lintig, J. (2012) Metabolism of carotenoids and retinoids related to vision. *J. Biol. Chem.*, **287**, 1627–1634.
30. Lindqvist, A., He, Y.G. and Andersson, S. (2005) Cell type-specific expression of beta-carotene 9′,10′-monooxygenase in human tissues. *J. Histochem. Cytochem.*, **53**, 1403–1412.
31. Kowatz, T., Babino, D., Kiser, P., Palczewski, K. and von Lintig, J. (2013) Characterization of human beta,beta-carotene-15,15′-monooxygenase (BCMO1) as a soluble monomeric enzyme. *Arch. Biochem. Biophys.*, **539**, 214–222.
32. Lietz, G., Oxley, A., Leung, W. and Hesketh, J. (2012) Single nucleotide polymorphisms upstream from the beta-carotene 15,15′-monoxygenase gene influence provitamin A conversion efficiency in female volunteers. *J. Nutr.*, **142**, 161S–165S.
33. van den Berg, H. (1999) Carotenoid interactions. *Nutr. Rev.*, **57**, 1–10.
34. Lobo, G.P., Hessel, S., Eichinger, A., Noy, N., Moise, A.R., Wyss, A., Palczewski, K. and von Lintig, J. (2010) ISX is a retinoic acid-sensitive gatekeeper that controls intestinal β, β-carotene absorption and vitamin A production. *FASEB J.*, **24**, 1656–1666.
35. Lobo, G.P., Amengual, J., Baus, D., Shivdasani, R.A., Taylor, D. and von Lintig, J. (2013) Genetics and diet regulate vitamin A production via the homeobox transcription factor ISX. *J. Biol. Chem.*, **288**, 9017–9027.
36. Choi, M.Y., Romer, A.I., Hu, M., Lepourcelet, M., Mechoor, A., Yesilaltay, A., Krieger, M., Gray, P.A. and Shivdasani, R.A. (2006) A dynamic expression survey identifies transcription factors relevant in mouse digestive tract development. *Development*, **133**, 4119–4129.
37. Cai, S.F., Kirby, R.J., Howles, P.N. and Hui, D.Y. (2001) Differentiation-dependent expression and localization of the class B type I scavenger receptor in intestine. *J. Lipid Res.*, **42**, 902–909.
38. Seino, Y., Miki, T., Kiyonari, H., Abe, T., Fujimoto, W., Kimura, K., Takeuchi, A., Takahashi, Y., Oiso, Y., Iwanaga, T. *et al.* (2008) Isx participates in the maintenance of vitamin A metabolism by regulation of beta-carotene 15,15′-monooxygenase (Bcmo1) expression. *J. Biol. Chem.*, **283**, 4905–4911.
39. Reboul, E. and Borel, P. (2011) Proteins involved in uptake, intracellular transport and basolateral secretion of fat-soluble vitamins and carotenoids by mammalian enterocytes. *Prog. Lipid Res.*, **50**, 388–402.
40. Amengual, J., Lobo, G.P., Golczak, M., Li, H.N., Klimova, T., Hoppel, C.L., Wyss, A., Palczewski, K. and von Lintig, J. (2011) A mitochondrial enzyme degrades carotenoids and protects against oxidative stress. *FASEB J.*, **25**, 948–959.
41. Palczewski, G., Amengual, J., Hoppel, C.L. and von Lintig, J. (2014) Evidence for compartmentalization of mammalian carotenoid metabolism. *FASEB J.*, **28**, 4457–4469.
42. Kiefer, C., Hessel, S., Lampert, J.M., Vogt, K., Lederer, M.O., Breithaupt, D.E. and von Lintig, J. (2001) Identification and characterization of a mammalian enzyme catalyzing the asymmetric oxidative cleavage of provitamin A. *J. Biol. Chem.*, **276**, 14110–14116.
43. Mein, J.R., Dolnikowski, G.G., Ernst, H., Russell, R.M. and Wang, X.D. (2010) Enzymatic formation of apo-carotenoids from the xanthophyll carotenoids lutein, zeaxanthin and beta-cryptoxanthin by ferret carotene-9′,10′-monooxygenase. *Arch. Biochem. Biophys.*, **506**, 109–121.

44. Hu, K.Q., Liu, C., Ernst, H., Krinsky, N.I., Russell, R.M. and Wang, X.D. (2006) The biochemical characterization of ferret carotene-9′,10′-monooxygenase catalyzing cleavage of carotenoids in vitro and in vivo. *J. Biol. Chem.*, **281**, 19327–19338.
45. Li, B., Vachali, P.P., Gorusupudi, A., Shen, Z., Sharifzadeh, H., Besch, B.M., Nelson, K., Horvath, M.M., Frederick, J.M., Baehr, W. *et al.* (2014) Inactivity of human β, β-carotene-9′,10′-dioxygenase (BCO2) underlies retinal accumulation of the human macular carotenoid pigment. *Proc. Natl Acad. Sci. USA*, **111**, 10173–10178.
46. Rigotti, A., Trigatti, B.L., Penman, M., Rayburn, H., Herz, J. and Krieger, M. (1997) A targeted mutation in the murine gene encoding the high density lipoprotein (HDL) receptor scavenger receptor class B type I reveals its key role in HDL metabolism. *Proc. Natl Acad. Sci. USA*, **94**, 12610–12615.
47. Hessel, S., Eichinger, A., Isken, A., Amengual, J., Hunzelmann, S., Hoeller, U., Elste, V., Hunziker, W., Goralczyk, R., Oberhauser, V. *et al.* (2007) CMO1 deficiency abolishes vitamin A production from beta-carotene and alters lipid metabolism in mice. *J. Biol. Chem.*, **282**, 33553–33561.
48. van Bennekum, A., Werder, M., Thuahnai, S.T., Han, C.H., Duong, P., Williams, D.L., Wettstein, P., Schulthess, G., Phillips, M.C. and Hauser, H. (2005) Class B scavenger receptor-mediated intestinal absorption of dietary beta-carotene and cholesterol. *Biochemistry*, **44**, 4517–4525.
49. Reboul, E., Klein, A., Bietrix, F., Gleize, B., Malezet-Desmoulins, C., Schneider, M., Margotat, A., Lagrost, L., Collet, X. and Borel, P. (2006) Scavenger receptor class B type I (SR-BI) is involved in vitamin E transport across the enterocyte. *J. Biol. Chem.*, **281**, 4739–4745.
50. Berg, C.J., LaFountain, A.M., Prum, R.O., Frank, H.A. and Tauber, M.J. (2013) Vibrational and electronic spectroscopy of the retro-carotenoid rhodoxanthin in avian plumage, solid-state films, and solution. *Arch. Biochem. Biophys.*, **539**, 142–155.
51. Amengual, J., Widjaja-Adhi, M.A., Rodriguez-Santiago, S., Hessel, S., Golczak, M., Palczewski, K. and von Lintig, J. (2013) Two carotenoid oxygenases contribute to mammalian provitamin A metabolism. *J. Biol. Chem.*, **288**, 34081–34096.
52. Bietrix, F., Yan, D., Nauze, M., Rolland, C., Bertrand-Michel, J., Comera, C., Schaak, S., Barbaras, R., Groen, A.K., Perret, B. *et al.* (2006) Accelerated lipid absorption in mice overexpressing intestinal SR-BI. *J. Biol. Chem.*, **281**, 7214–7219.
53. Acton, S., Rigotti, A., Landschulz, K.T., Xu, S., Hobbs, H.H. and Krieger, M. (1996) Identification of scavenger receptor SR-BI as a high density lipoprotein receptor. *Science*, **271**, 518–520.
54. Borel, P., Preveraud, D. and Desmarchelier, C. (2013) Bioavailability of vitamin E in humans: an update. *Nutr. Rev.*, **71**, 319–331.
55. Borel, P., Desmarchelier, C., Nowicki, M., Bott, R., Morange, S. and Lesavre, N. (2014) Interindividual variability of lutein bioavailability in healthy men: characterization, genetic variants involved, and relation with fasting plasma lutein concentration. *Am. J. Clin. Nutr.*, **100**, 168–175.
56. Borel, P., Moussa, M., Reboul, E., Lyan, B., Defoort, C., Vincent-Baudry, S., Maillot, M., Gastaldi, M., Darmon, M., Portugal, H. *et al.* (2009) Human fasting plasma concentrations of vitamin E and carotenoids, and their association with genetic variants in apo C-III, cholesteryl ester transfer protein, hepatic lipase, intestinal fatty acid binding protein and microsomal triacylglycerol transfer protein. *Br. J. Nutr.*, **101**, 680–687.
57. Borel, P., Moussa, M., Reboul, E., Lyan, B., Defoort, C., Vincent-Baudry, S., Maillot, M., Gastaldi, M., Darmon, M., Portugal, H. *et al.* (2007) Human plasma levels of vitamin E and carotenoids are associated with genetic polymorphisms in genes involved in lipid metabolism. *J. Nutr.*, **137**, 2653–2659.
58. Nassif, N.T., Lobo, G.P., Wu, X., Henderson, C.J., Morrison, C.D., Eng, C., Jalaludin, B. and Segelov, E. (2004) PTEN mutations are common in sporadic microsatellite stable colorectal cancer. *Oncogene*, **23**, 617–628.
59. von Lintig, J., Kreusch, D. and Schroder, J. (1994) Opine-regulated promoters and LysR-type regulators in the nopaline (noc) and octopine (occ) catabolic regions of Ti plasmids of Agrobacterium tumefaciens. *J. Bacteriol.*, **176**, 495–503.